

Luminescent ruthenium polypyridyl complexes with extended 'dppz' like ligands as DNA targeting binders and cellular agents

Bjørn C. Poulsen, Sandra Estalayo-Adrián, Salvador Blasco, Sandra A. Bright,^a John M. Kelly, D. Clive Williams and Thorfinnur Gunnlaugsson

Electronic Supplementary Information

1. Synthesis

1.1. Synthesis of ligands

Synthesis of 1,10-phenanthroline-5,6-dione.¹ To a mixture of 1,10-phenanthroline (1.03 g, 5.73 mmol, 1 eq) and KBr (5.02 g, 42.2 mmol, 7 eq) cold concentrated H₂SO₄ (20 ml, 95%) was added drop-wise followed by drop-wise addition of cold concentrated HNO₃ (8 ml, 65%). The reaction mixture was heated at 80 °C for one hour followed by heating at 100 °C for further four hours. The mixture was cooled to room temperature, and let stir overnight. The mixture was reheated to 100 °C and purged with nitrogen to remove bromine gas. After cooling to room temperature the mixture was poured over ice (1 L), 6 M NaOH (50 ml) was added followed by addition of NaHCO₃ until pH of the mixture was between 5 and 7. The precipitate was removed by filtration, and the filtrate was extracted using CH₂Cl₂ (4 x 100 ml). The combined CH₂Cl₂ layers were washed with H₂O (3 x 100 ml), and the solvent was evaporated leaving a brown yellow solid. The final product was obtained as a yellow solid by recrystallization from methanol (0.88 g, 73%). *m.p.*: > 250 °C (Lit. > 250 °C).¹ ¹H NMR (CDCl₃, 400 MHz, δ): 9.10 (2H, dd, *J* = 4.7 Hz, 1.8 Hz), 8.48 (2H, dd, *J* = 7.9 Hz, 1.8 Hz), 7.58 (2H, dd, *J* = 7.9 Hz, 4.7 Hz). ¹³C NMR (CDCl₃, 100 MHz, δ): 178.76 (C=O), 156.50, 153.00 (q), 137.42, 128.18 (q), 125.72. IR (ATR, cm⁻¹): 3062 (aromatic C-H stretch), 1684 (C=O stretch), 1413 and 1293 (C-N stretches). ESI-HRMS (*m/z*) calculated for C₁₂H₇N₂O₂: 211.0508. Found: 211.0501 [M+H]⁺.

Synthesis of 2-methyl-6-nitroquinoxaline.² A solution of 4-nitro-1,2-benzenediamine (10.00 g, 64.45 mmol, 1 eq) in ethanol (500 ml) was heated to reflux. Aqueous methylglyoxal (40%, 15 ml, 99 mmol, 1.5 eq) was added, and the resulting solution was refluxed for two hours. The reaction mixture was cooled to room temperature. The solvent was removed at reduced pressure, and the resulting solid was dissolved in CH₂Cl₂ (200 ml) and washed with H₂O (3 x 100 ml). The CH₂Cl₂ phase was filtered through SiO₂ (100 ml), eluted with CH₂Cl₂ (200 ml), and the combined organic phase was evaporated. The solid is recrystallized three times from isopropanol, and the product was isolated as white crystals (5.32 g, 43%). *m.p.*: 163-166 °C (Lit. 168-169 °C).³ ¹H NMR (DMSO-*d*₆, 400 MHz, δ): 9.06 (1H, s), 8.85 (1H, d, *J* = 2.6 Hz), 8.52 (1H, dd, *J* = 9.2 Hz, 2.6 Hz), 8.22 (1H, d, *J* = 9.2 Hz), 2.78 (3H, s, CH₃). ESI-HRMS (*m/z*) calculated for C₉H₆N₃O₂: 188.0460. Found: 188.0462 [M-H]⁻.

Synthesis of 2-methyl-5-amino-6-nitroquinoxaline. Metallic sodium (1.46 g, 63.4 mmol, 4 eq) was added to anhydrous methanol (250 ml) at room temperature. The sodium reacted with methanol resulting in the formation of hydrogen gas. Hydroxylammonium chloride (2.10 g, 30.2 mmol, 2 eq) was added to the solution. The mixture was stirring for one hour. 2-Methyl-6-nitroquinoxaline (3.00 g, 15.8 mmol, 1 eq) was added to the colourless solution immediately yielding a green-yellow mixture. The solution was stirring overnight forming a dark mixture. To the mixture was added concentrated aqueous NH_4NO_3 (25 ml). The solvent was removed at reduced pressure. The solid was dissolved in CH_2Cl_2 (300 ml) and washed with H_2O (3 x 100 ml). The CH_2Cl_2 layer was dried over MgSO_4 before the solvent was removed at reduced pressure. The resulting solid was purified using automatic column chromatography (120 g SiO_2 , hexane:EtOAc 100:0 to 70:30). The product 2-methyl-5-amino-6-nitroquinoxaline was obtained as a yellow solid (0.870 g, 27%). Calculated for $\text{C}_9\text{H}_8\text{N}_4\text{O}_2$: C, 52.94; H, 3.95; N, 27.44%. Found: C, 53.05; H, 3.92; N, 26.72%. *m.p.*: 182-183 °C. ^1H NMR ($\text{DMSO}-d_6$, 400 MHz, δ): 8.82 (1H, s), 8.42 (2H, s, NH_2), 8.23 (1H, d, $J = 9.6$ Hz), 7.07 (1H, d, $J = 9.6$ Hz), 2.72 (3H, s, CH_3). ^{13}C NMR ($\text{DMSO}-d_6$, 100 MHz, δ): 158.15 (q), 145.10 (q), 145.06 (q), 143.93, 131.87 (q), 125.96, 125.76 (q), 114.03, 22.16 (CH_3). IR (ATR, cm^{-1}): 3358 (N-H stretch), 1611 (N-H bend), 1503 (C- NO_2), 1305 (C- NO_2).

Synthesis of 2-methyl-5,6-diaminoquinoxaline.⁴ 2-Methyl-5-amino-6-nitroquinoxaline (0.87 g, 4.3 mmol, 1 eq) and 10% Pd/C (0.16 g) were suspended in ethanol (100 ml). The mixture was heated at reflux for 30 minutes followed by addition of hydrazine monohydrate (4 ml, 85 mmol, 20 eq). The mixture turned brown. After two hour the hot mixture was filtered through a path of celite (1 cm), and after extraction with CH_2Cl_2 (20 ml) the solvent was removed at reduced pressure. The product 2-methyl-5,6-diaminoquinoxaline was obtained as a blood red solid (0.68 g, 91%). *m.p.*: 177-178 °C. ^1H NMR ($\text{DMSO}-d_6$, 400 MHz, δ): 8.50 (1H, s), 7.19 (1H, d, $J = 8.7$ Hz), 7.09 (1H, d, $J = 8.7$ Hz), 5.10 (2H, s, NH_2), 5.07 (2H, s, NH_2), 2.57 (3H, s, CH_3).

Synthesis of 4-nitro-2,1,3-benzothiadiazole.⁵ A solution of 4-nitro-1,2-benzenediamine (5.00 g, 32.7 mmol, 1 eq) and triethylamine (7.70 ml, 55.2 mmol, 1.7 eq) in DMF (50 ml) was cooled to 0°C. Thionyl chloride (5.7 ml, 78.6 mmol, 2.4 eq) was added drop-wise and the reaction mixture was stirred at 0°C for 2 hours. The mixture was quenched with H_2O and extracted with CH_2Cl_2 . The organic layer was washed with a saturated solution of NaHCO_3 , water and brine and dried with MgSO_4 . Solvent was removed at reduced pressure. The obtained solid was purified by silica chromatography using CH_2Cl_2 :hexane (1:1) as eluent yielding a yellow solid which was dried *in vacuo* (3.03 g, 51%). ^1H NMR (CDCl_3 , 400 MHz, δ): 8.99 (1H, s), 8.44 (1H, d, $J = 9.5$ Hz), 8.17 (1H, d, $J = 9.5$ Hz).

Synthesis of 5-amino-4-nitro-2,1,3-benzothiadiazole.^{6, 7} A suspension of 5-nitro-2,1,3-benzothiadiazole (1.01g, 5.58 mmol, 1 eq) and hydroxylammonium chloride (1.01 g, 14.6 mmol, 2.6 eq) in ethanol (50 ml) was cooled to 0°C. A saturated ethanolic solution of KOH (10 ml) was added drop-wise to the cold mixture. The reaction mixture was stirred for 2 hours and then quenched with HCl 36%. The resulting yellow precipitate was filtered, washed with ethanol and used directly in the

next reaction. ^1H NMR (CDCl_3 , 400 MHz, δ): 13.60 (2H, s, NH_2), 12.95 (1H, d, $J = 9.9$ Hz), 11.92 (1H, d, $J = 9.8$ Hz).

Synthesis of 4,5-diamine-2,1,3-benzothiadiazole.^{6, 7} To a boiling mixture of 4-amino-5-nitro-2,1,3-benzothiadiazole in water (50 ml), $\text{Na}_2\text{S}_2\text{O}_4$ (5.24 g, 30.1 mmol) was added slowly. The reaction mixture was stirred for 20 minutes and filtered while hot. The filtrate was cooled at room temperature overnight and the resulting red precipitate was washed with cold H_2O and dried *in vacuo* (659 mg, 71%). ^1H NMR ($\text{DMSO-}d_6$, 400 MHz, δ): 7.25 (1H, d, $J = 9.1$ Hz), 7.17 (1H, d, $J = 9.0$ Hz), 5.09 (2H, s, NH_2), 4.93 (2H, s, NH_2).

1.2. Synthesis of complexes

Synthesis of dichloro(1,5-cyclooctadiene)ruthenium(II).⁸ Ruthenium(III) chloride hydrate (2.01 g, 7.69 mmol, 1 eq) and 1,5-cyclooctadiene (18.5 ml, 151 mmol, 20 eq) was mixed in ethanol (200 ml). The solution was degassed with argon for about 10 minutes. The mixture was refluxed for three days followed by cooling to room temperature. The brown precipitate was isolated by filtration, washed with ethanol (75 ml) and dried *in vacuo* (2.09 g, 97%). *m.p.*: > 250 °C (Lit. > 250 °C).⁸

Procedure 1: Synthesis of $[\text{Ru}(\text{L})_2\text{Cl}_2]$ complexes.⁹ The appropriate polypyridyl ligand (**phen** or **TAP**, 2 eq) and $[\text{Ru}(\text{cod})\text{Cl}_2]_n$ (1 eq) were suspended in DMF (10 mL). The mixture was degassed by bubbling with nitrogen for 15 minutes and then heated at 140 °C for 40 minutes using microwave irradiation. The mixture was cooled to room temperature, it was mixed with Me_2CO (25 ml), and left overnight at -15 °C. The product was isolated by filtration as a black solid which was washed with cold Me_2CO (10 ml) and dried *in vacuo*.

Synthesis of bis(1,10-phenanthroline)ruthenium(II)chloride.⁹ The complex $[\text{Ru}(\text{phen})_2\text{Cl}_2]$ was synthesized according to standard **Procedure 1** using 1,10-phenanthroline (496 mg, 2.75 mmol, 2 eq) and $[\text{Ru}(\text{cod})\text{Cl}_2]_n$ (386 mg, 1.38 mmol, 1 eq) yielding the product as a dark purple powder (468 mg, 64%). *m.p.*: > 250 °C (Lit. > 250 °C).⁹ ^1H NMR ($\text{DMSO-}d_6$, 400 MHz, δ): 10.28 (2H, dd, $J = 5.3$ Hz, 1.3 Hz); 8.71 (2H, dd, $J = 8.2$ Hz, 1.3 Hz); 8.29 (2H, d, $J = 8.9$ Hz); 8.24 (2H, dd, $J = 8.0$ Hz, 1.1 Hz); 8.21 (2H, dd, $J = 8.2$ Hz, 5.3 Hz); 8.14 (2H, d, $J = 8.9$ Hz); 7.75 (2H, dd, $J = 5.4$ Hz, 1.1 Hz); 7.33 (2H, dd, $J = 8.0$ Hz, 5.4 Hz).

Synthesis of bis(1,4,5,8-tetraazaphenanthrene)ruthenium(II)chloride.⁹ The complex $[\text{Ru}(\text{TAP})_2\text{Cl}_2]$ was synthesized according to standard **Procedure 1** using **TAP** (287 mg, 1.58 μmol , 2 eq) and $[\text{Ru}(\text{cod})\text{Cl}_2]_n$ (220 mg, 0.785 μmol , 1 eq) yielding the product as a dark purple powder (361 mg, 85%). *m.p.*: > 250 °C (Lit. > 250 °C).⁹ ^1H NMR ($\text{DMSO-}d_6$, 400 MHz, δ): 10.18 (2H, d, $J = 2.7$ Hz), 9.48 (2H, d, $J = 2.6$ Hz), 8.62 (4H, m), 8.48 (2H, d, $J = 9.4$ Hz), 8.32 (2H, d, H_6 , $J = 2.7$ Hz). MALDI-HRMS (m/z) calculated for $\text{C}_{20}\text{H}_{12}\text{N}_8\text{RuCl}_2$: 535.9605. Found: 535.9631 $[\text{M}]^+$.

2. Characterization

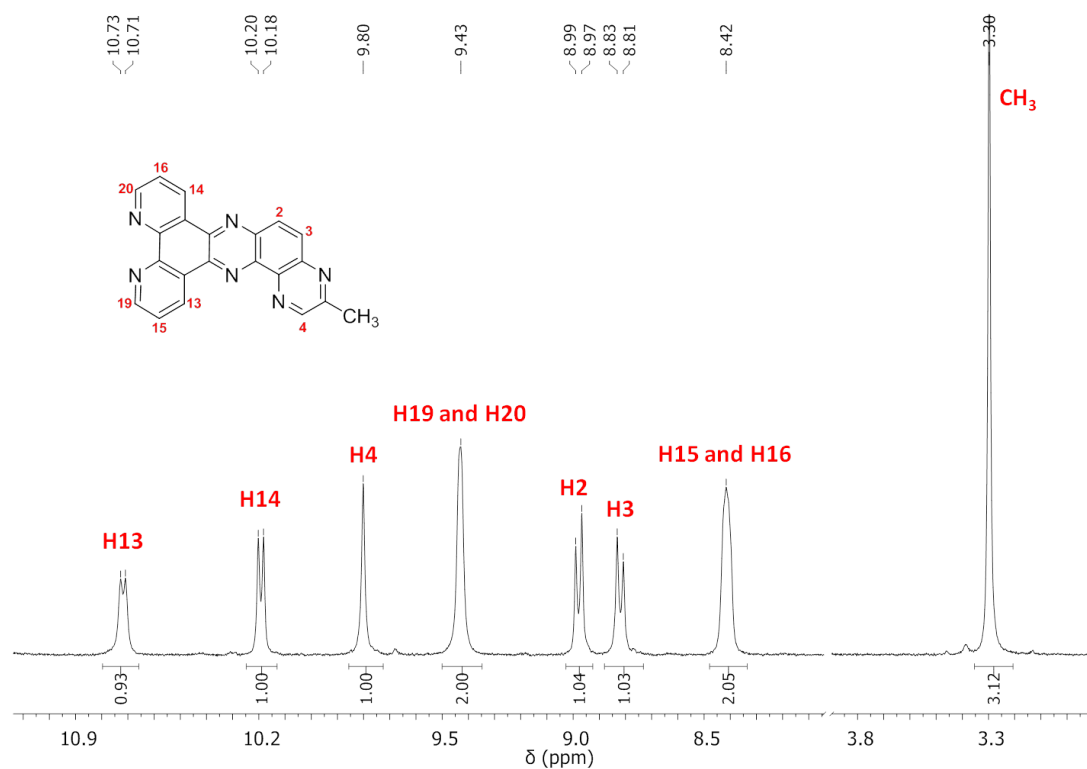


Figure S1: ¹H-NMR (CDCl₃/TFA, 400 MHz) spectrum of 3-methylpyrazino[2,3-h]dipyrido[3,2-a:2',3'-c]phenazine (**mpdppz**).

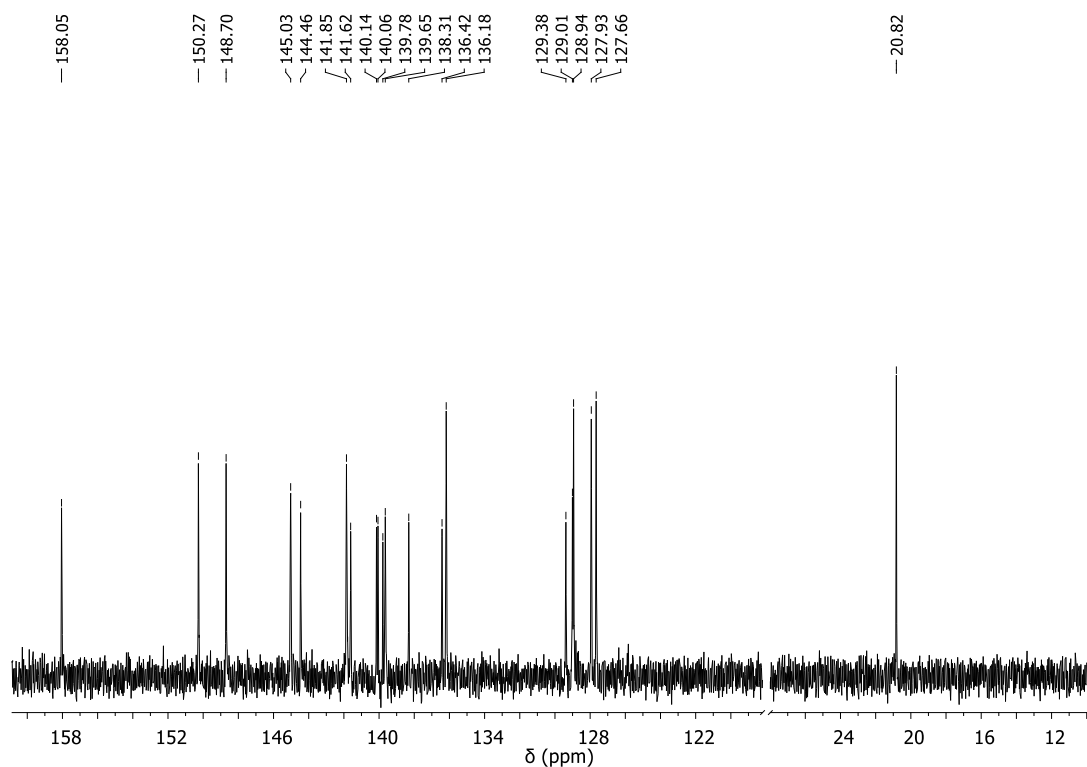


Figure S2: ¹³C-NMR (CDCl₃/TFA, 100 MHz) spectrum of 3-methylpyrazino[2,3-h]dipyrido[3,2-a:2',3'-c]phenazine (**mpdppz**).

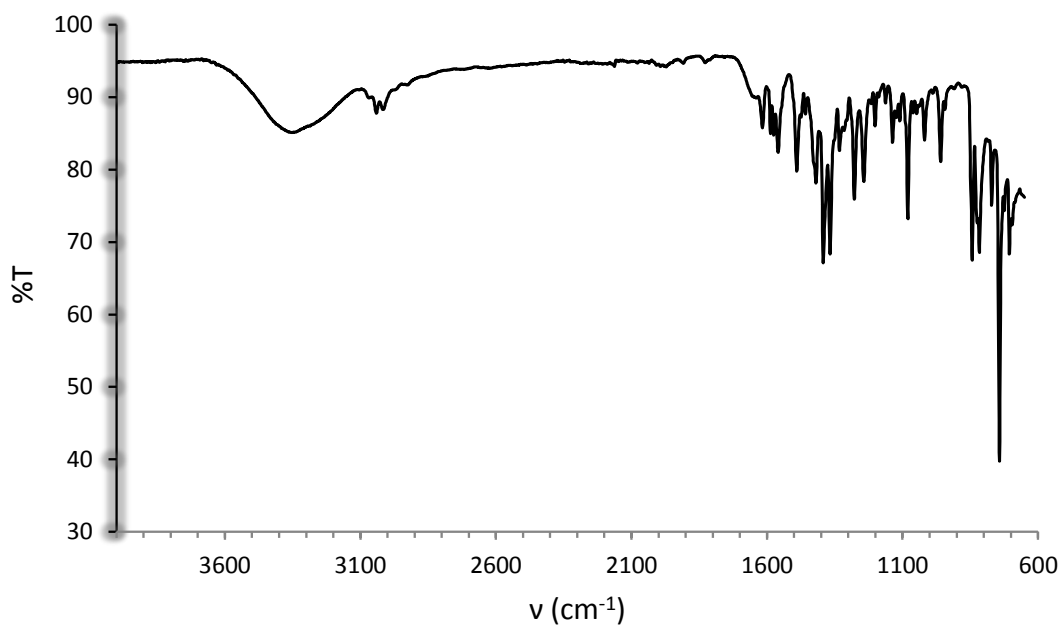


Figure S3: IR spectrum of 3-methylpyrazino[2,3-h]dipyrido[3,2-a:2',3'-c]phenazine (**mpdppz**).

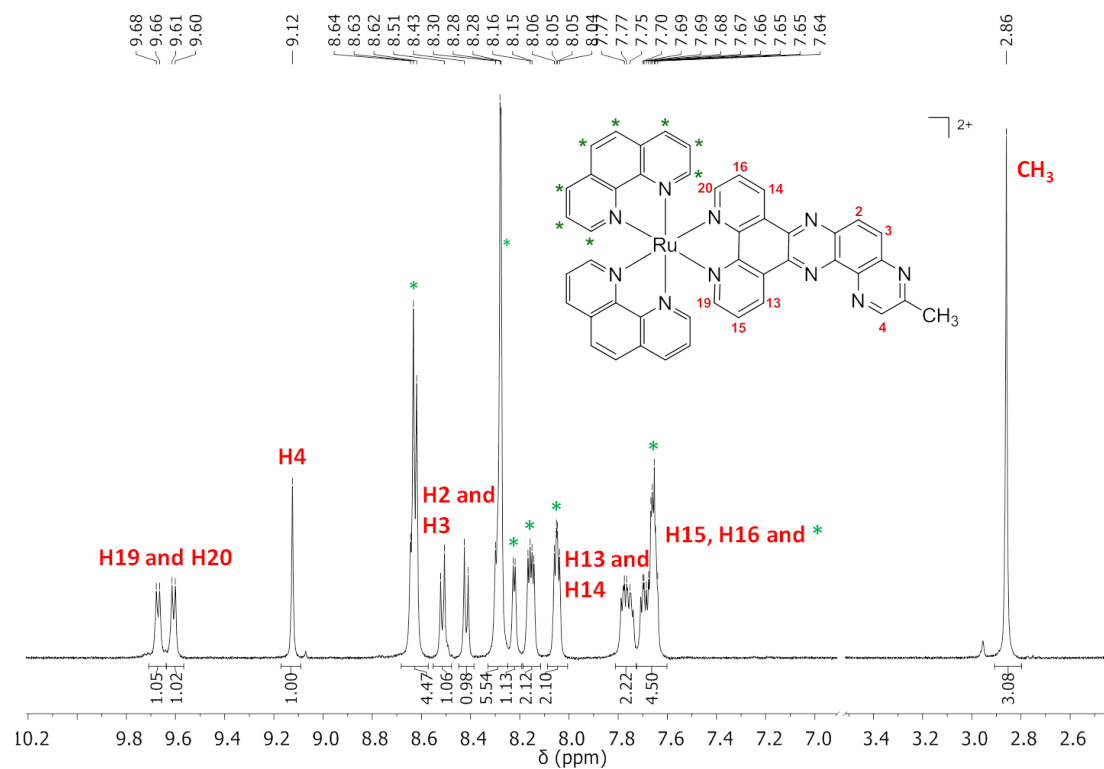


Figure S4: ¹H-NMR (CD₃CN, 400 MHz) spectrum of complex **3**.

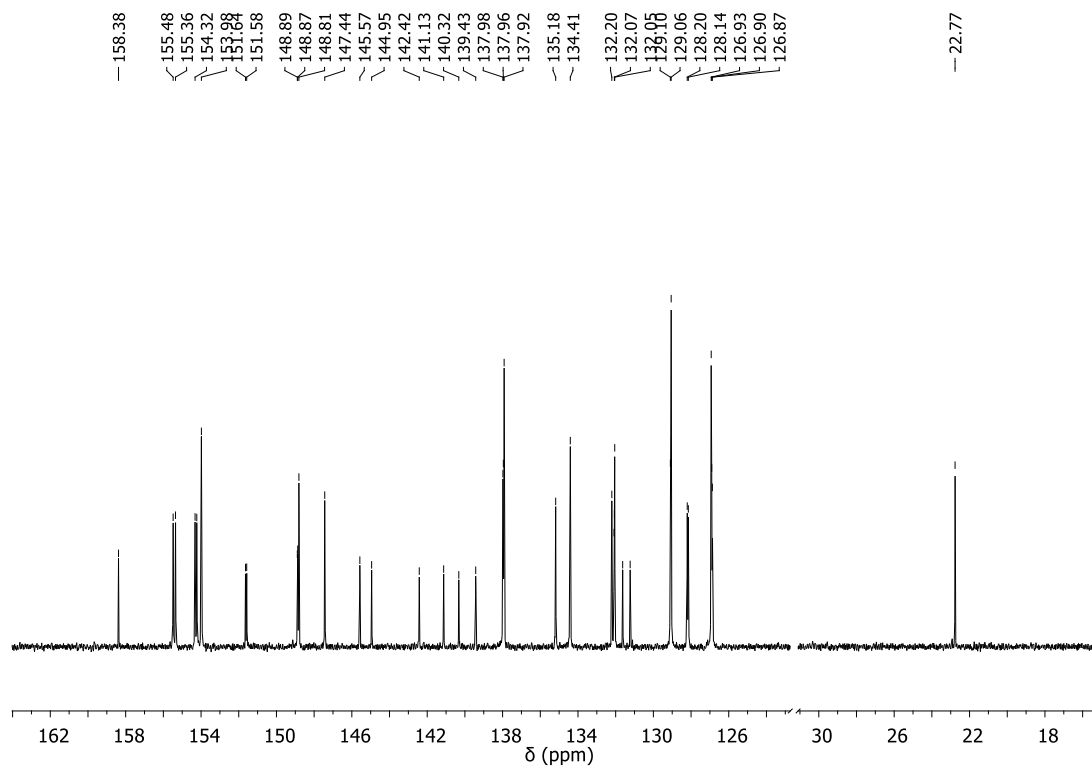


Figure S5: ^{13}C -NMR (CD_3CN , 100 MHz) spectrum of complex **3**.

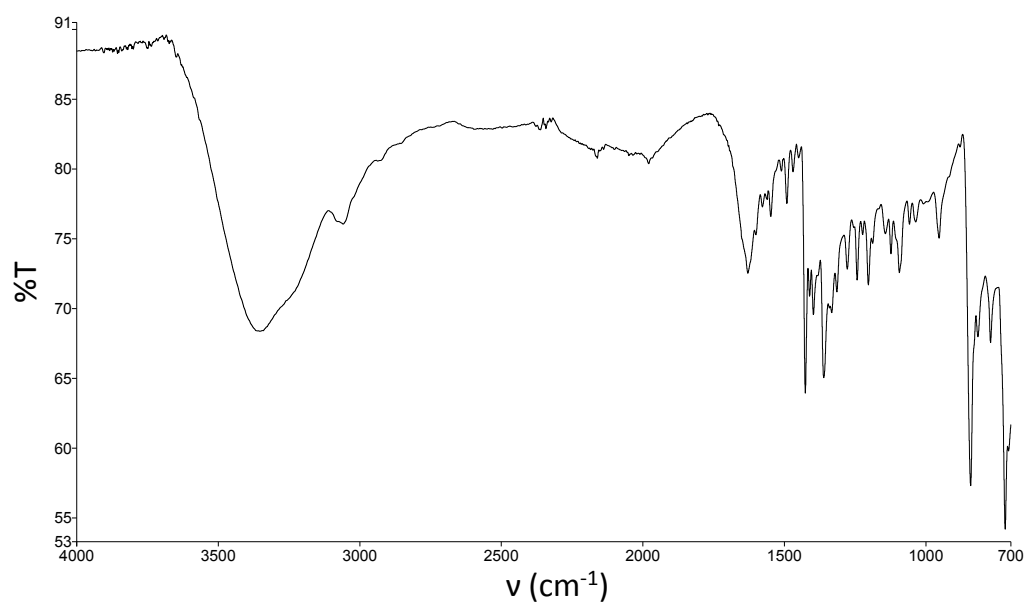


Figure S6: IR spectrum of complex **3**.

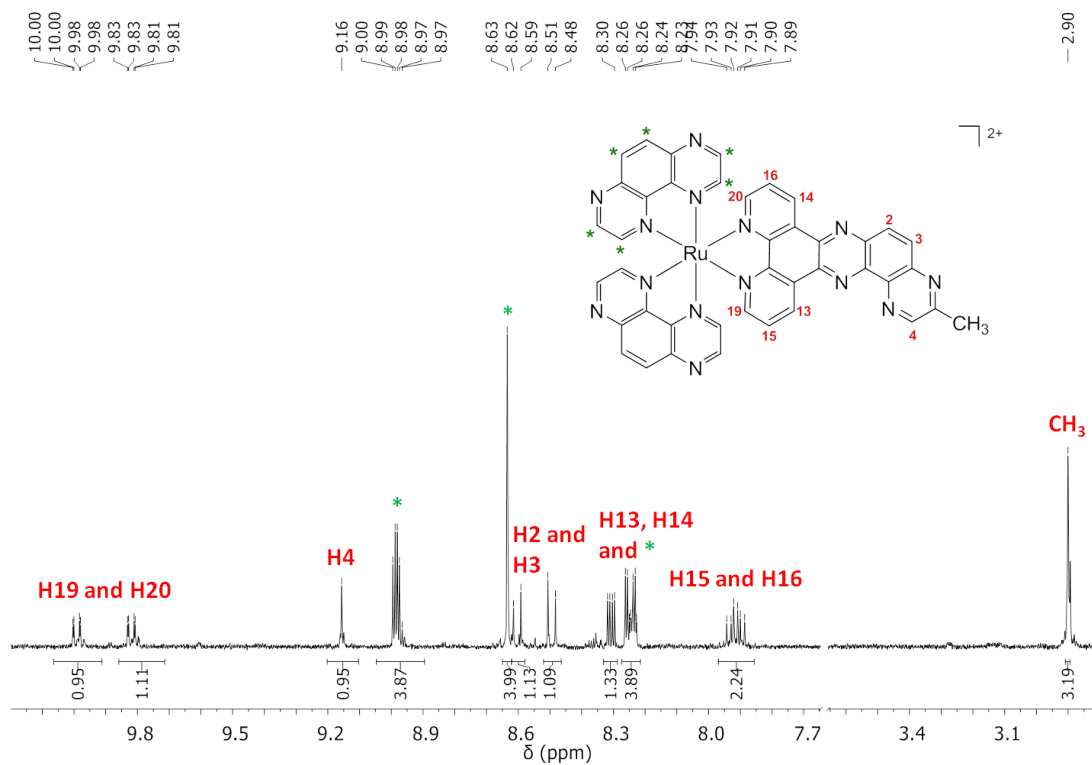


Figure S7: ¹H-NMR (CD₃CN, 400 MHz) spectrum of complex 4.

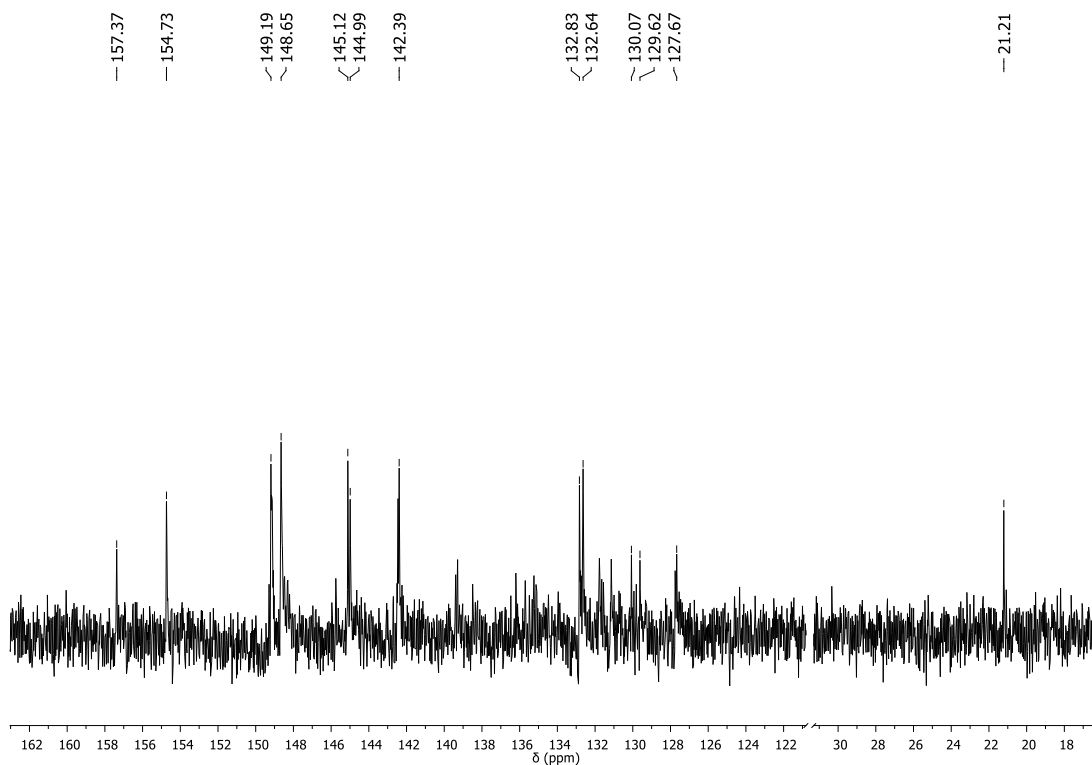


Figure S8: ¹³C-NMR (D₂O, 100 MHz) spectrum of complex 4.

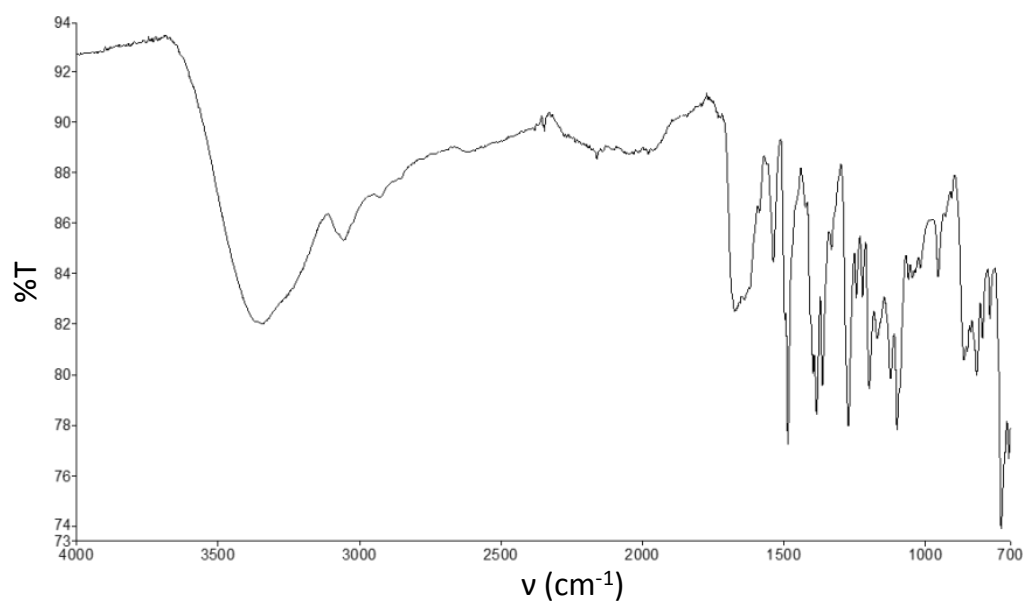


Figure S9: IR spectrum of complex 4.

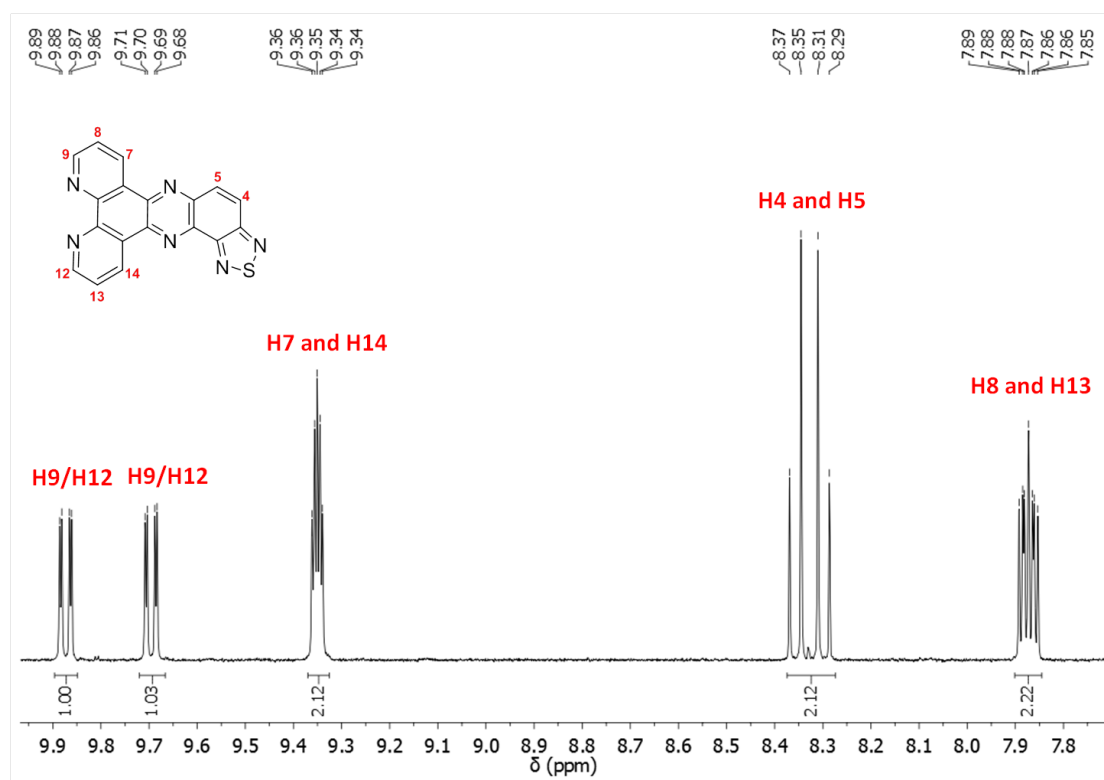


Figure S10: $^1\text{H-NMR}$ (CDCl_3 , 400 MHz) of dipyrido[3,2-a:2',3'-c][1,2,5]thiadiazolo[3,4-4,3]phenazine (dtp).

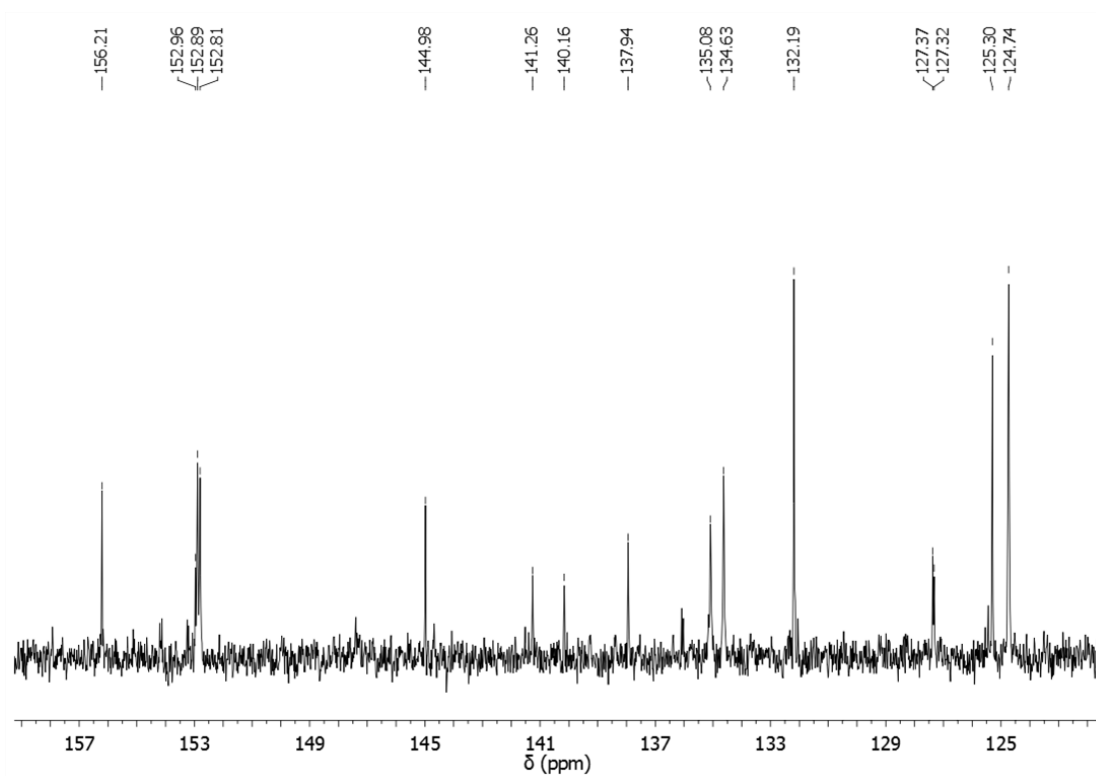


Figure S11: ^{13}C -NMR (CDCl_3 , 100 MHz) spectrum of dipyrido[3,2-a:2',3'-c][1,2,5]thiadiazolo[3,4-4,3]phenazine (**dtp**).

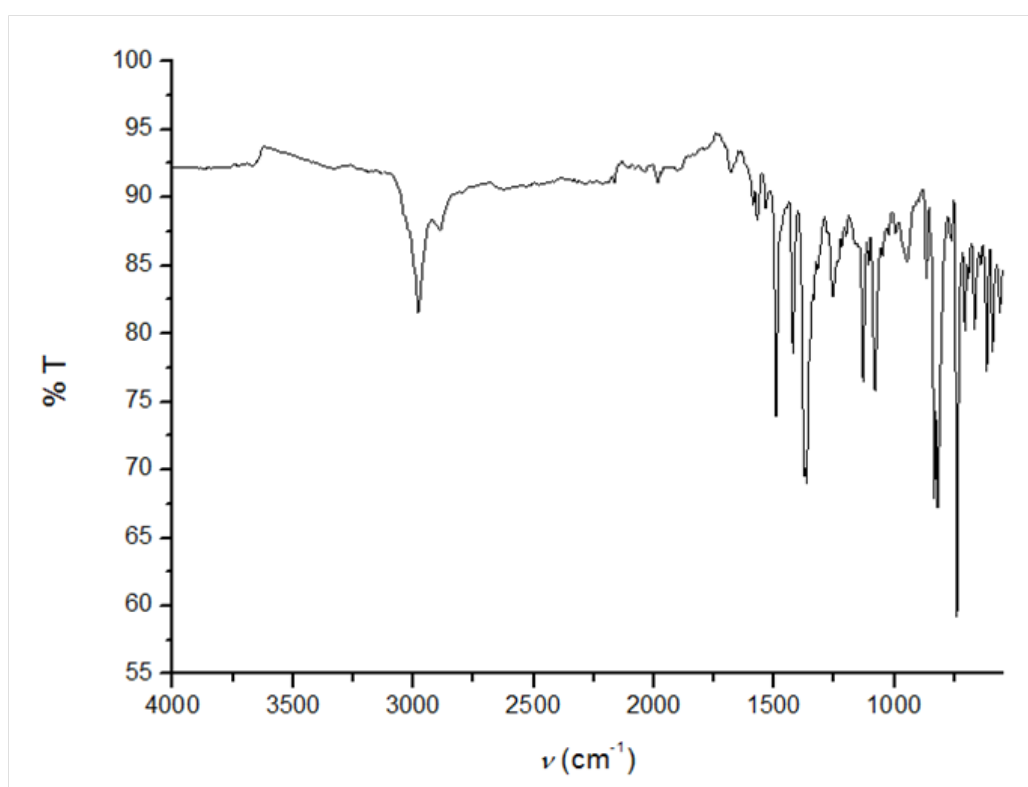


Figure S12: IR spectrum of dipyrido[3,2-a:2',3'-c][1,2,5]thiadiazolo[3,4-4,3]phenazine (**dtp**).

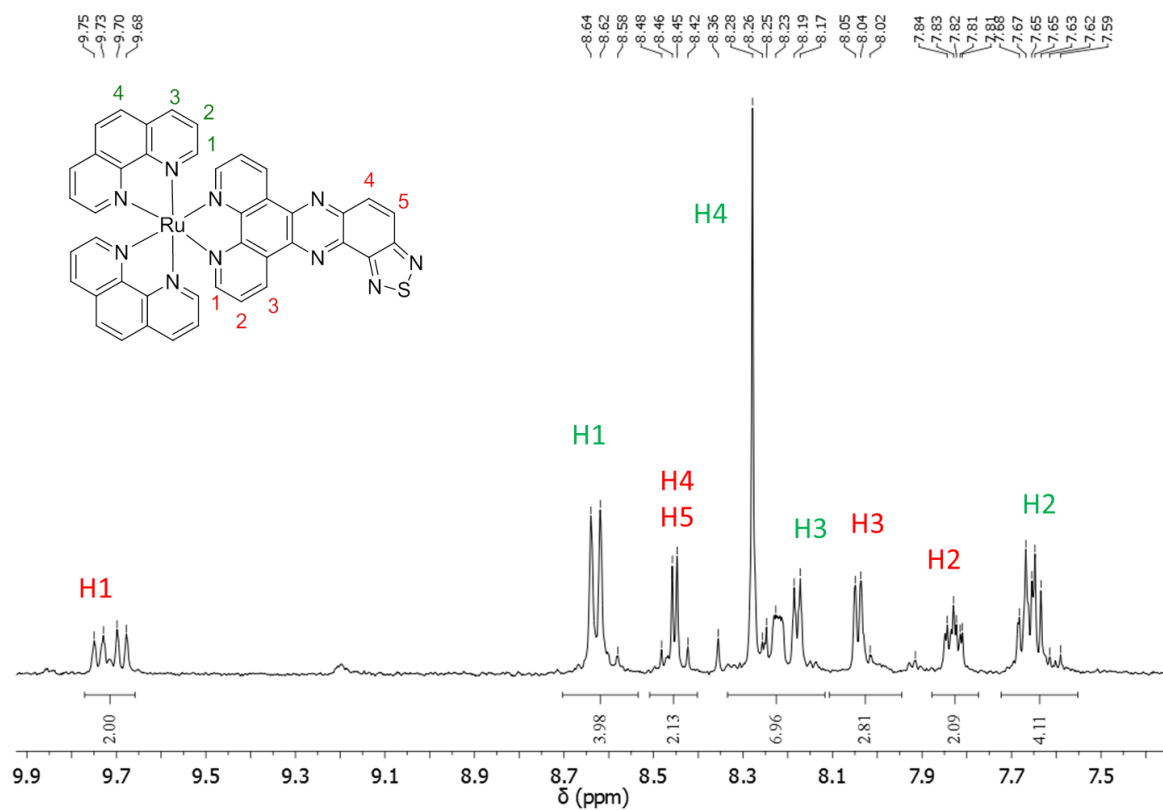


Figure S13: $^1\text{H-NMR}$ (CD_3CN , 400 MHz) of complex 5.

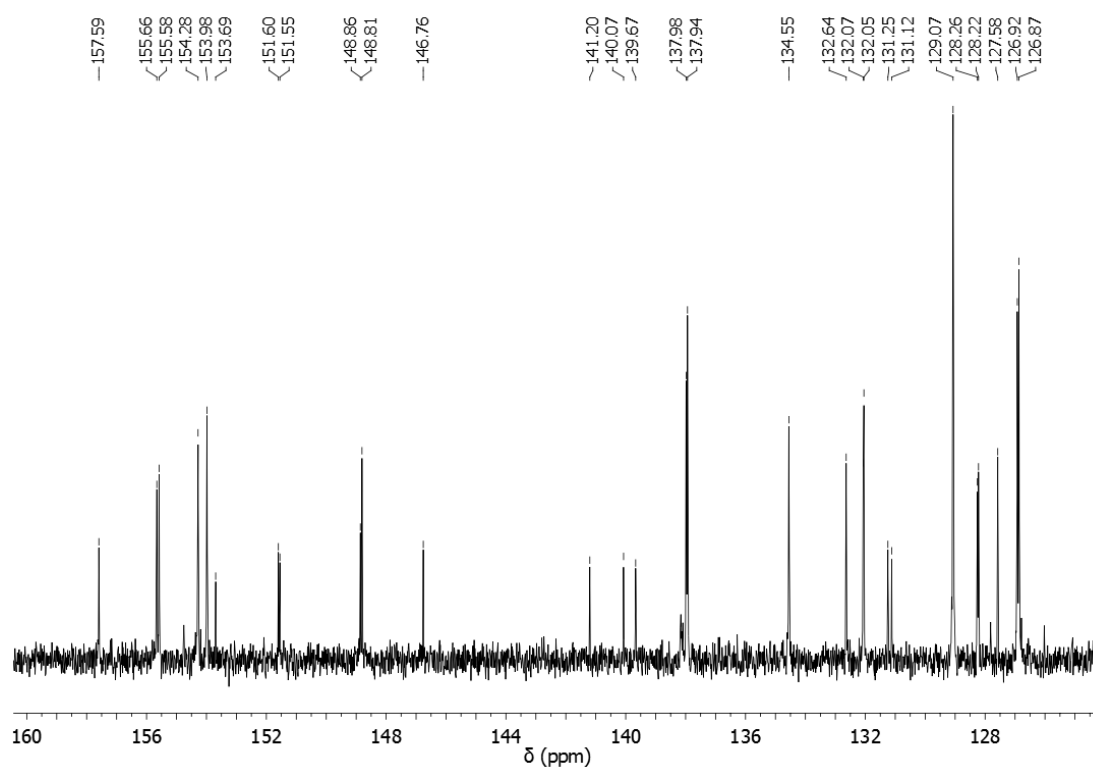


Figure S14: $^{13}\text{C-NMR}$ (CD_3CN , 100 MHz) of complex 5.

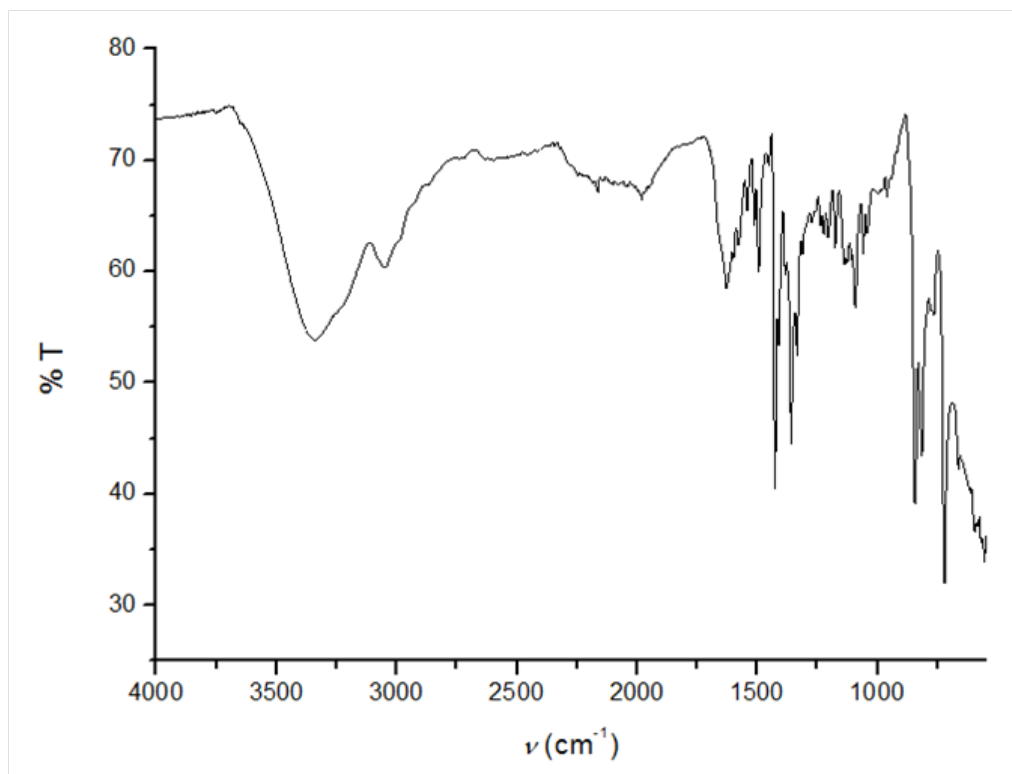


Figure S15: IR spectrum of complex 5.

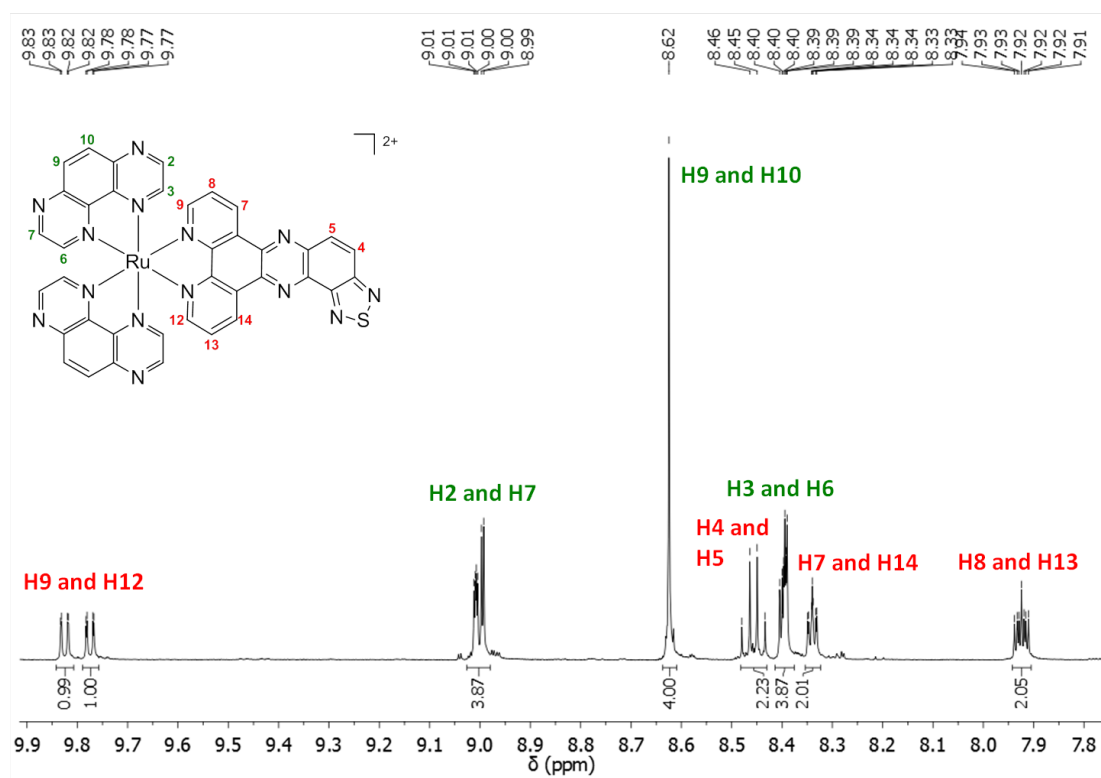


Figure S16: $^1\text{H-NMR}$ (CD_3CN , 600 MHz) of complex 6.

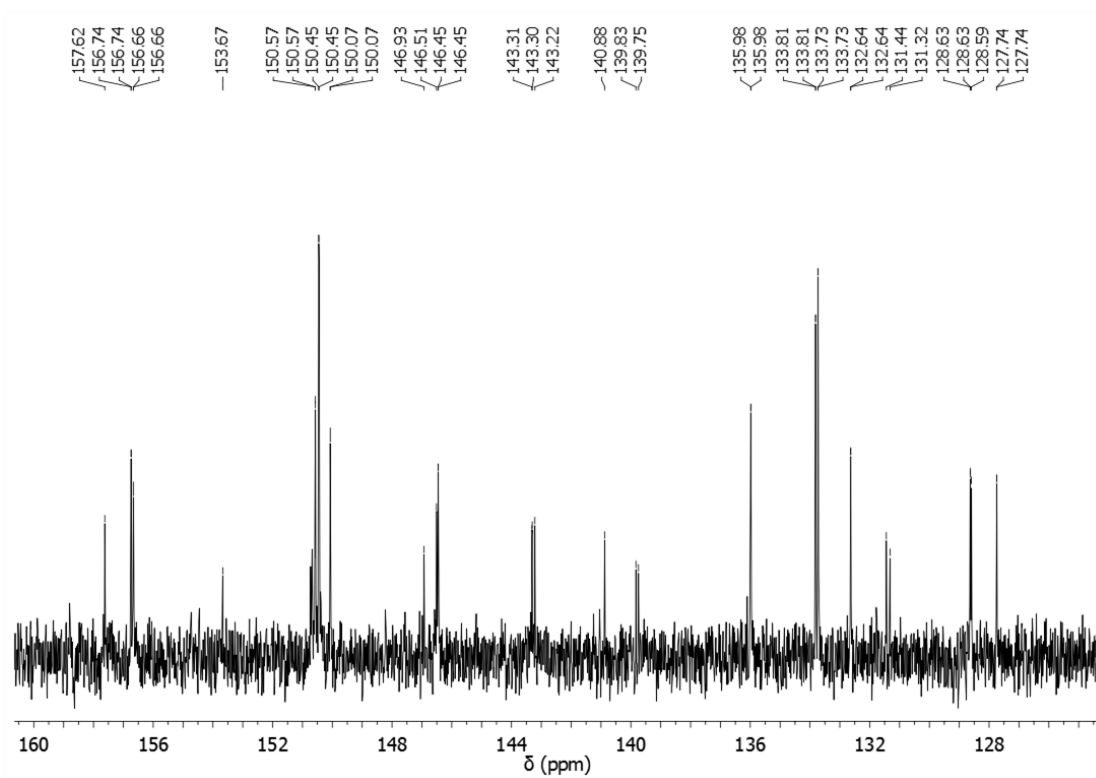


Figure S17: ^{13}C -NMR (CD_3CN , 100 MHz) of complex **6**.

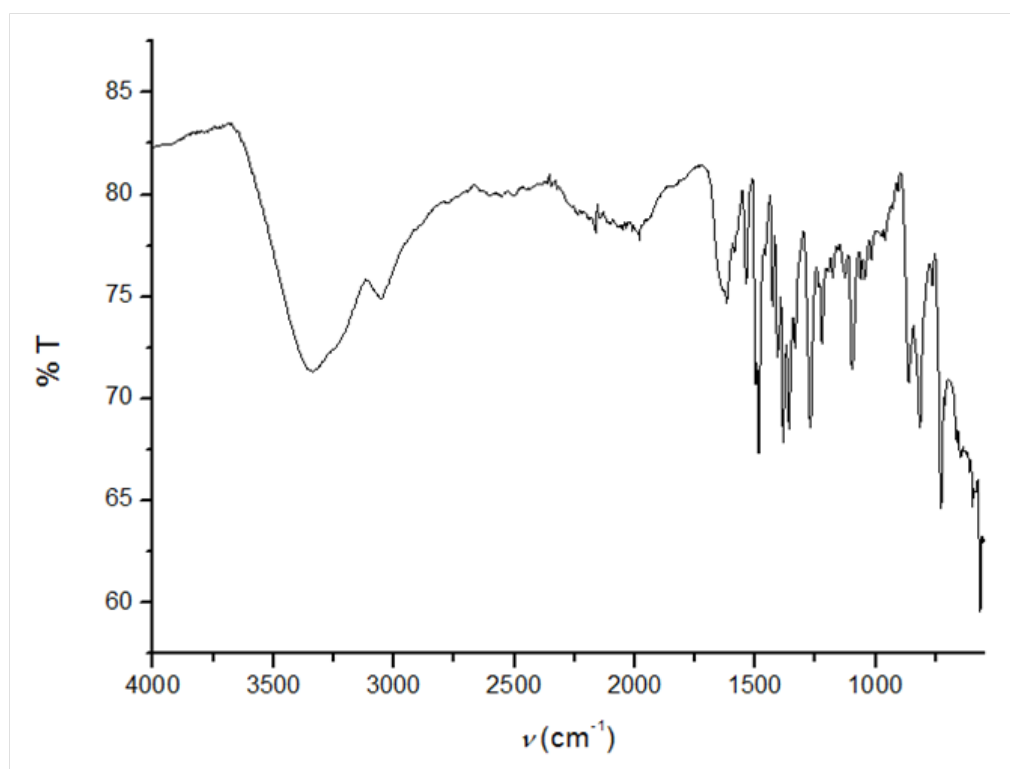


Figure S18: IR spectrum of complex **6**.

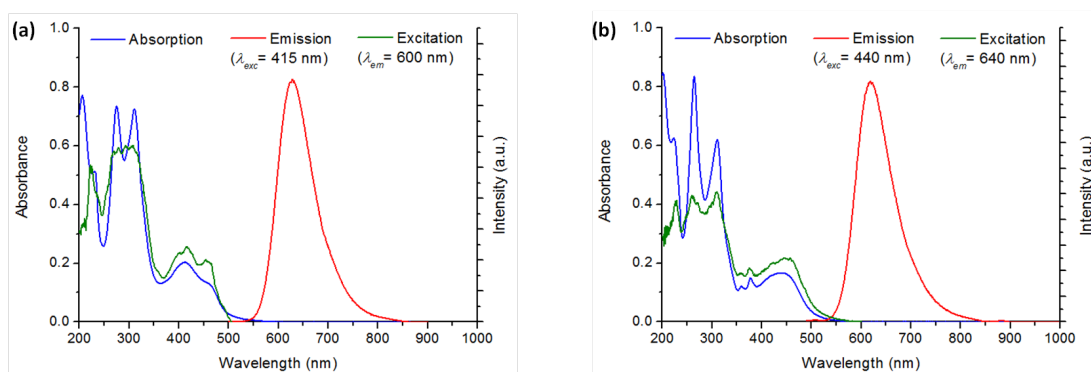


Figure S19: UV-Vis absorption, emission and excitation spectra of complexes (a) **4** in acetonitrile and (b) **5** in 10 mM phosphate buffered aqueous solution at pH 7.4.

Extinction coefficients determination

The extinction coefficients were determined in the following manner: absorptions were measured at different concentrations of complex, and absorptions were plotted against concentrations. The extinction coefficients were derived from the slope coefficients of the best linear fits of these plots. In every case the statistical error, corresponding to a 95% confidence interval, was calculated from the standard error and the appropriate t-distribution.

Luminescence quantum yields

The luminescence quantum yields were calculated relative to the literature value of $[\text{Ru}(\text{bpy})_3]^{2+}$ (0.028 in H_2O).¹⁰ The quantum yields were determined from the integration of fluorescence spectra obtained in the reference solvent. The spectra were obtained under the same conditions using a solution of the same absorbance and excited at the same wavelength.

3. DNA binding studies

a) Absorption and emission titrations with DNA

A modification of a method by Carter, Rodriguez and Bard was used to calculate the binding constant (K_b) for the affinity of the complexes to DNA and the binding site size (n) in number of base pairs occupied by one complex at binding.¹¹ Their binding model presumes that the interaction between a ligand and DNA can be described by the following mass-action equation:

$$K_b = \frac{C_b}{C_f \cdot C_{site}} \quad (\text{S3.1})$$

Here C_f represents the actual concentration of free complex and C_b the concentration of complex bound to DNA. C_{site} represents the concentration of “free binding sites” defined from the total concentration of DNA measured in base pairs (C_{bp}) as:

$$C_{site} = C_{bp}/n - C_b \quad (S3.2)$$

In this way it is presumed that DNA contains fixed binding sites that can be interpreted as independent species. The assumption would only be fully valid if the binding sites were fixed, if all binding sites had the same affinity for complex, and that there was no cooperativity. By combining equation (S3.1) and (S3.2) the following expression is obtained:

$$C_b = \frac{b - (b^2 - 4 \cdot K_b^2 C_t C_{bp}/n)^{0.5}}{2K_b}$$

$$b = 1 + K_b C_t + K_b C_{bp}/n$$

C_b can be determined from the absorption and emission data if a well-defined molar response for free and bound complex exists. If the molar absorption or emission for free complex (e_f) and for bound complex (e_b) is known the concentration of bound complex can be determined from the relative change in the absorption or emission:

$$C_b = \frac{e_a - e_f}{e_b - e_f} \cdot C_t \quad (S3.3)$$

Here C_t is the total concentration of complex and e_a represent the apparent molar absorptivity ($\epsilon_a = A/C_t$) or apparent molar emission ($E_a = Em/C_t$). Combining these two expression gives following well known equation:

$$\frac{e_a - e_f}{e_b - e_f} = \frac{b - (b^2 - 4 \cdot K_b^2 C_t C_{bp}/n)^{0.5}}{2K_b C_t} \quad (S3.4)$$

In the cases where e_f and e_b are known the binding parameters K_b and n can be calculated by fitting the parameters in the equation to a plot of $(e_a - e_f)/(e_b - e_f)$ (fraction of all complex bound to DNA) as dependent variable and with C_{bp} and C_t as independent variable. In the absorption and emission titration carried out the change in C_t is only a result of dilution at addition of DNA.

e_f is a quantity that usually can be measured directly from the absorption or emission before addition of DNA when the total concentration of complex is known. It is more difficult to obtain an accurate value of e_b since, to measure this, all complexes need to bind to DNA, which theoretically and practically will only be the case at infinite concentration of DNA. Usually the molar response for bound complex is found by calculating the absorption or emission at high concentration of DNA in which case the fraction of complexes bound to DNA is close to 100%. This method will in general result in a small overestimate of the amount of bound complex and a corresponding underestimate of the amount of free complex. The concentration of free complex is low at the end of the titration, and even a small underestimate of its value can result in a value that is a small fraction of the true concentration. Since the mass-action equation used to calculate K_b is a fraction containing C_f in the numerator a decrease

in C_f to, for example, a tenth of its true value will give a corresponding ten-fold overestimation of the binding constant.

In the case of a weak binding the main problem will be to reach a point in the titration at which almost all complex is bound resulting in a larger overestimate of the calculated value of C_b . In our case in which the binding is strong the binding constant is exceptionally dependent on the points of the titration curve that correspond to almost 100% binding. For those points a small error in e_b will have a fairly large impact on the size of K_b that easily become twice as big (see figure S20).

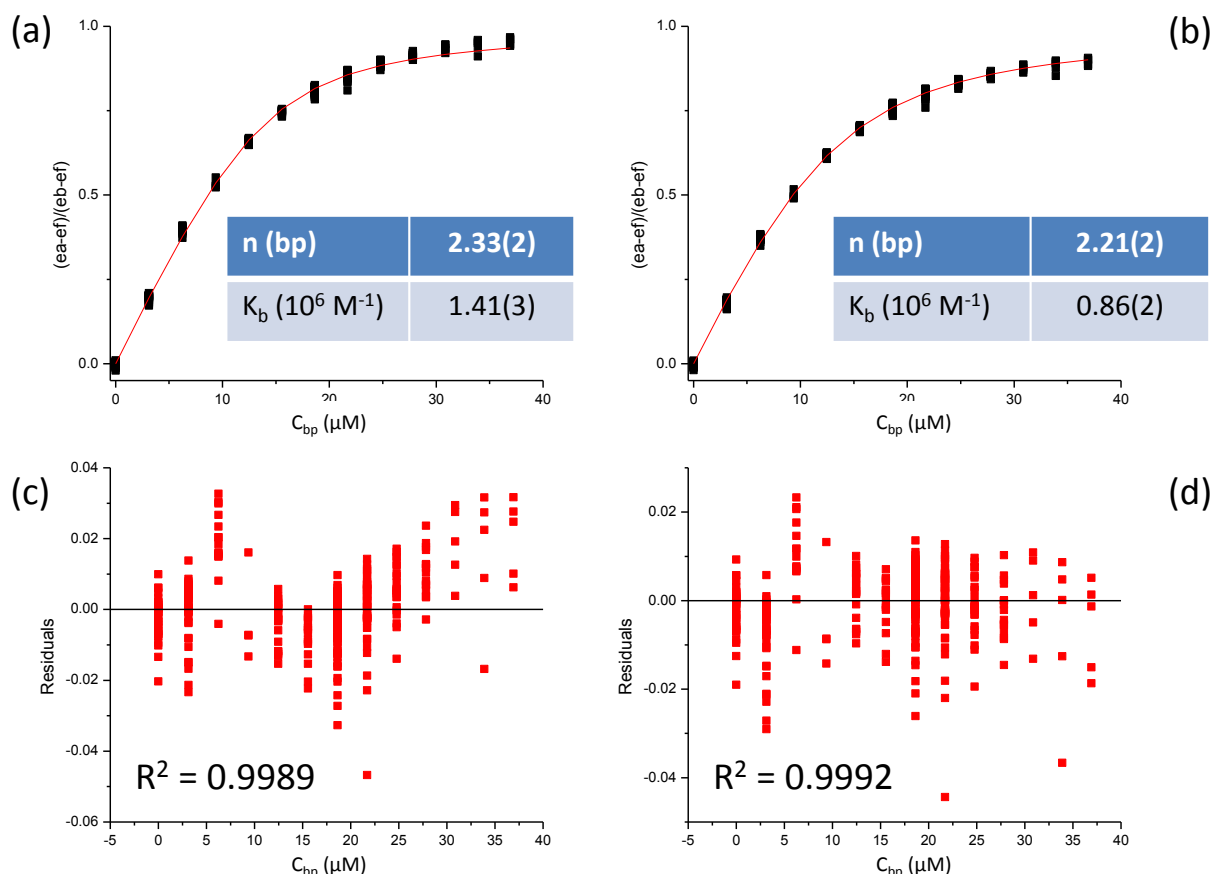


Figure S20: Fit of n and K_b in equation (S3.4) to a plot of $(\varepsilon_a - \varepsilon_f)/(\varepsilon_b - \varepsilon_f)$ against C_{bp} for compound **4** in 10 mM sodium phosphate buffered solution with 160 mM NaCl. Several measurements were obtained for each concentration to obtain high precision.¹² (a) Plot calculated with ε_b estimated as ε_a for high concentration of DNA (P/D about 30). (b) Plot where ε_b is fitted to give the best fit of equation (S3.4) by use of equation (S3.5) below. ε_b in (b) is only 1.0% lower than ε_b in (a), but K_b is almost 50% lower. (c) and (d) show residuals for the two situations (a) and (b) respectively and the corresponding R^2 values. The R^2 values are very close to 1 for both plots, but the residuals in (c) are systematically positive at the end of the titration whereas in (d) they are randomly distributed around zero.

We have addressed those issues by a small rewriting of the classical equation (S3.4):

$$e_a = \frac{b - (b^2 - 4 \cdot K_b^2 C_t C_{bp} / n)^{0.5}}{2K_b C_t} \times (e_b - e_f) + e_f$$

(S3.5)

Here e_b can be fitted together with n and K_b and it is no longer necessary to measure an approximated value (see figure S21). It will also be possible to fit e_f in the equation. This should in general be unnecessary since e_f can be calculated directly from the absorption or emission before addition of DNA. However, even in this case the measured value of e_f can be associated with errors (e.g. random errors and variations in baseline), and it has been decided to use a fitted value of e_f .

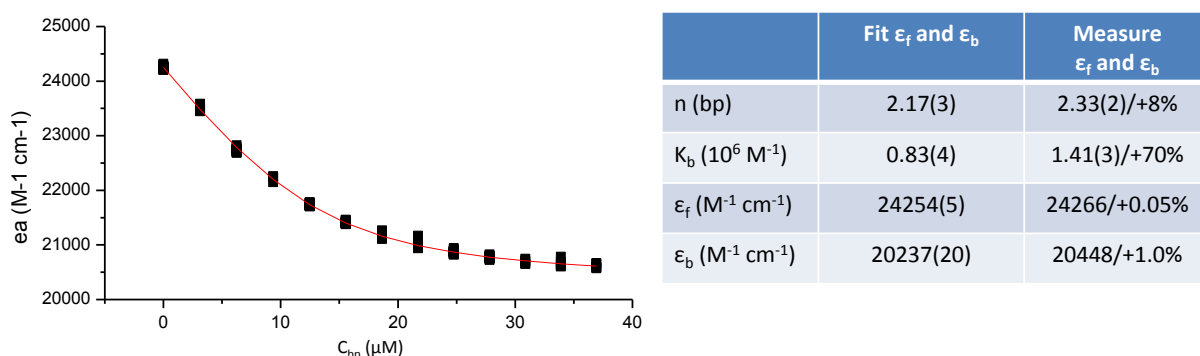


Figure S21: Fit of ϵ_f and ϵ_b together with n and K_b in equation (S3.5) to plot of ϵ_a against C_{bp} (x-axis) and C_t (not shown) for compound **4** in 10 mM sodium phosphate buffered solution with 160 mM NaCl. The table compares the values obtained from this method with those obtained in figure S20 (a) including how much these values differ from the values obtained with our method.

Similar approaches are known from simple equilibria between monovalent or divalent species.¹⁴ In a method by Bujalowski *et al.* it has been shown how the concentration profile for binding to DNA can be calculated in a fully model independent manner, however this method demands several independent titrations to be carried out.¹⁵

The data processing program OriginPro 8.5¹³ has been used to calculate the binding parameters by fitting n , K_b , e_f and e_b in the equation above. In these fits e_a for absorption or emission is the dependent parameter and C_{bp} and C_t are the independent parameters. In presentations of plots and fits in the paper have only been shown the dependence of C_{bp} (see figure S20). Prior to fitting have for the emission data of complex **3** and **5** been deleted points that from equation (S3.3) would give unphysical concentration profile. In phosphate buffered solution at low ionic strength do this refer to decrease in the emission after reaching a maximum (would correspond to decrease in C_b at increase in C_{bp} , see figure S22). For pure water in addition have been deleted points in the beginning of the titration curve corresponding to positive curvature.

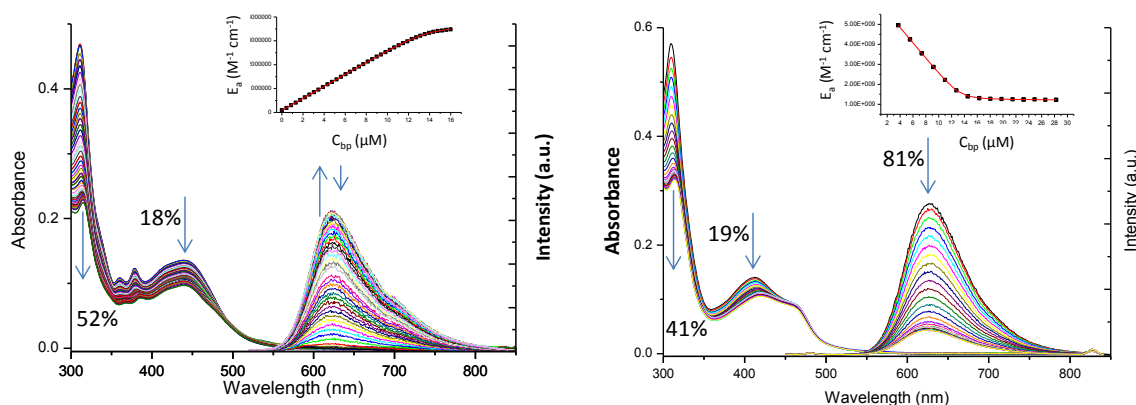


Figure S22: Changes in the UV-Vis and emission spectra of **5** (left) and **6** (right) with the addition of increasing amounts of st-DNA (0-100 μM) at pH 7.4 (10 mM sodium phosphate). Inset: Plot for emission data of E_a at increasing C_{bp} and the corresponding non-linear fit of equation (S3.5). Similar plots and fits have been made for the absorption data.

Table S1: Binding parameters obtained from absorption data for the binding between the complexes and st-DNA in 10 mM sodium phosphate buffered solution at pH 7.4 and either with or without 160 mM NaCl (high and low ionic strength, respectively). The parameters and the standard errors of the last significant digits (in bracket) are for the means of three replicates.

	Low ionic strength		High ionic strength	
	K_b (10^6 M^{-1})	n (#bp)	K_b (10^6 M^{-1})	n (#bp)
3	2.9(2)	1.67(7)	1.5(4)	2.31(6)
4	13(2)	1.69(5)	0.68(7)	1.70(83)
5	13(5)	1.35(4)	1.8(4)	1.99(5)
6	6(1)	1.63(1)	0.58(8)	1.63(3)

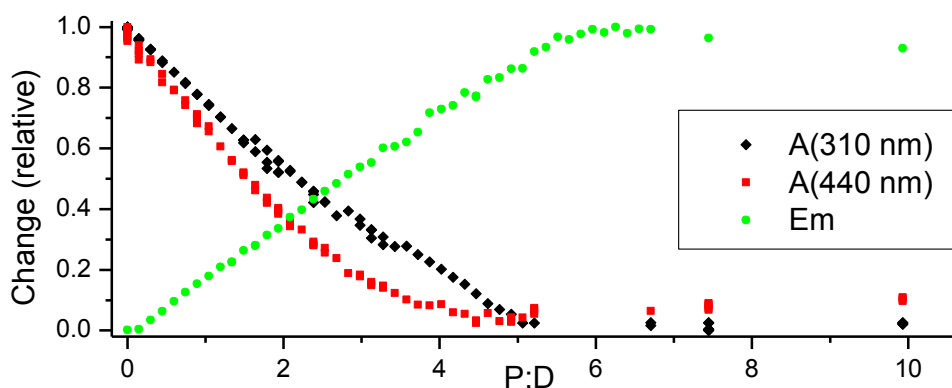


Figure S23: Comparison of the relative change of the apparent molar response for absorption at 310 nm and at 440 nm and in the integrated emission at increasing concentration of st-DNA to complex **3** in 10 mM sodium phosphate buffered solution at pH 7.4.

Table S2: Comparison of the binding parameters obtained from the absorption and emission data for the binding of complex **3** and st-DNA in 10 mM sodium phosphate buffered solution at pH 7.4. The calculated value of n is larger when the value was calculated from the absorbance at 310 nm and from the emission compared to the value calculated from the absorbance at 440 nm.

	Abs (440 nm)		Abs (310 nm)		Emission	
	K_b ($10^6 M^{-1}$)	n (#bp)	K_b ($10^6 M^{-1}$)	n (#bp)	K_b ($10^6 M^{-1}$)	n (#bp)
3	2.9(2)	1.67(7)	7(2)	2.17(4)	27(4)	2.50(8)

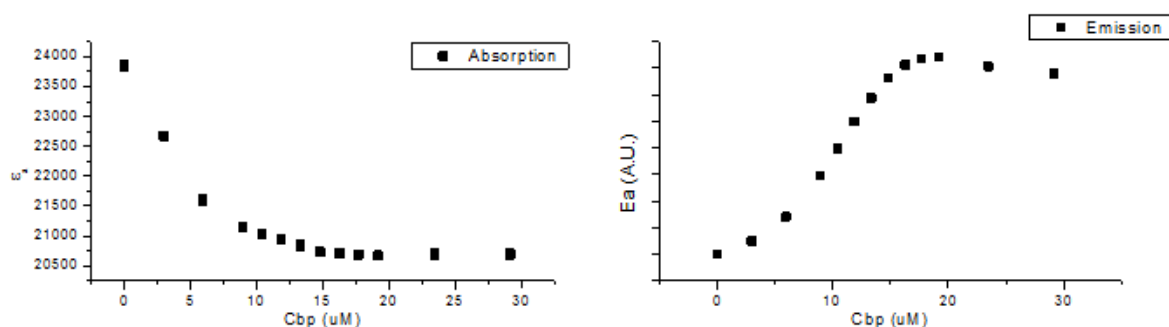


Figure S24: Changes in the UV-Vis and emission spectra of **3** in pure water with the addition of increasing amounts of st-DNA with no other ionic species present other than DNA and the compound itself. The pH value is ca. 6 (not buffered solution).

Table S3: Binding parameters obtained from absorption and emission data for the binding of complex **3** and st-DNA in pure water with no other ionic species present other than DNA and the compound itself.

	Absorption		Emission	
	K_b ($10^6 M^{-1}$)	n (#bp)	K_b ($10^6 M^{-1}$)	n (#bp)
3	0.8(2)	1.04(8)	81(9)	2.84(1)

b) Circular dichroism studies

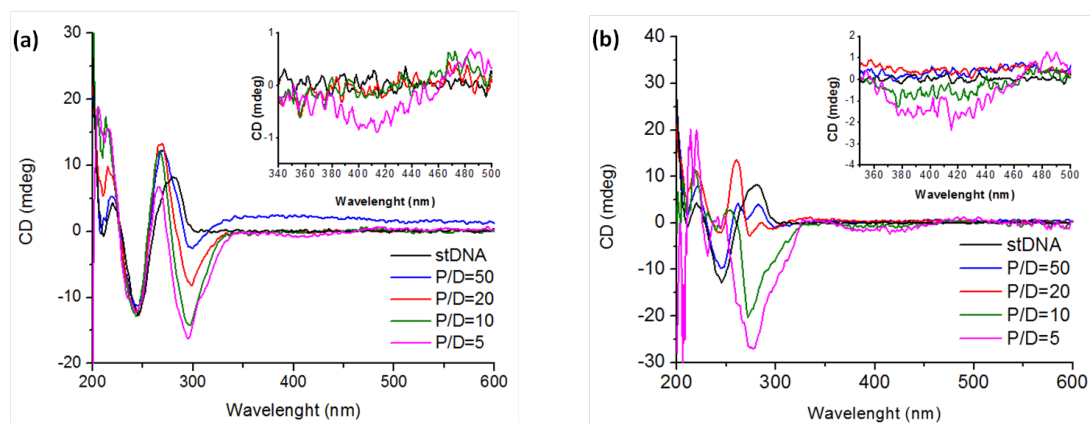
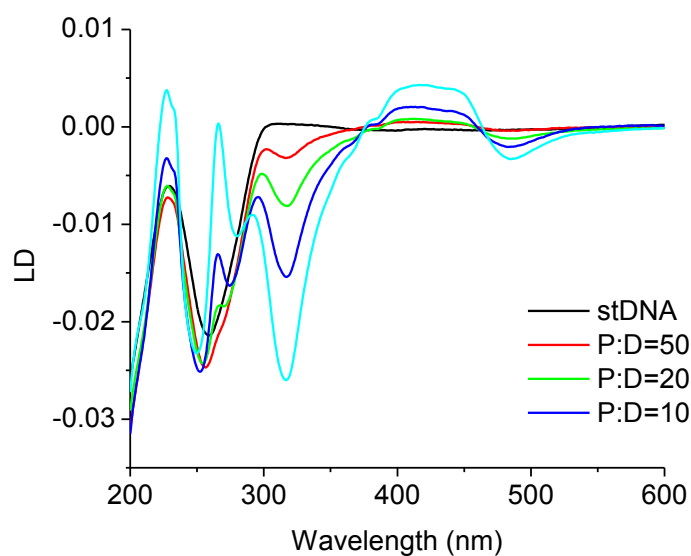


Figure S25: Circular dichroism spectra of st-DNA (150 μM) in 10 mM sodium phosphate buffered aqueous solution at pH 7.4, in the absence and presence of (a) **4** and (b) **5** at different P/D ratios.

c) Linear dichroism studies

(a) $[\text{Ru}(\text{phen})_2\text{mpdppz}]^{2+}$



(b) $[\text{Ru}(\text{TAP})_2\text{mpdppz}]^{2+}$

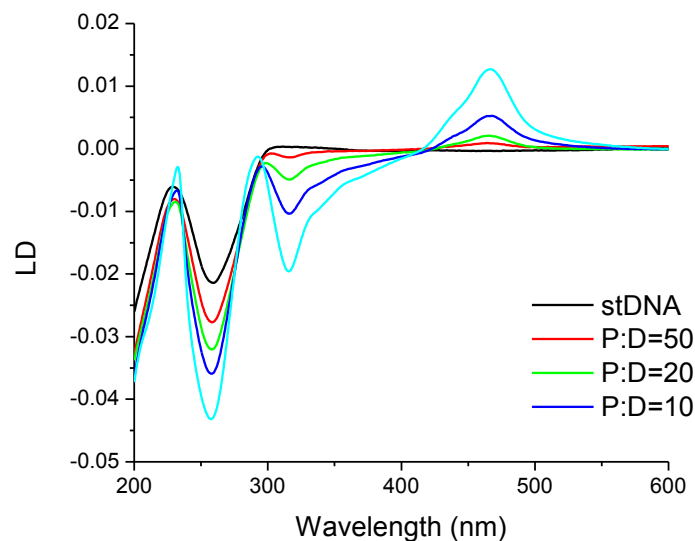
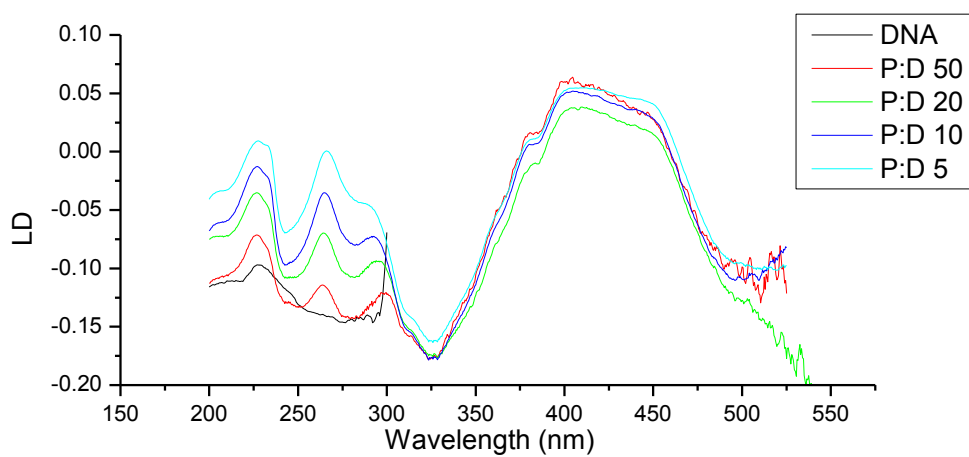


Figure S26: Linear dichroism spectra of st-DNA (400 μM) in 10 mM sodium phosphate buffered aqueous solution at pH 7.4, in the absence and presence of (a) **3** and (b) **4** at different P/D ratios.

(a)



(b)

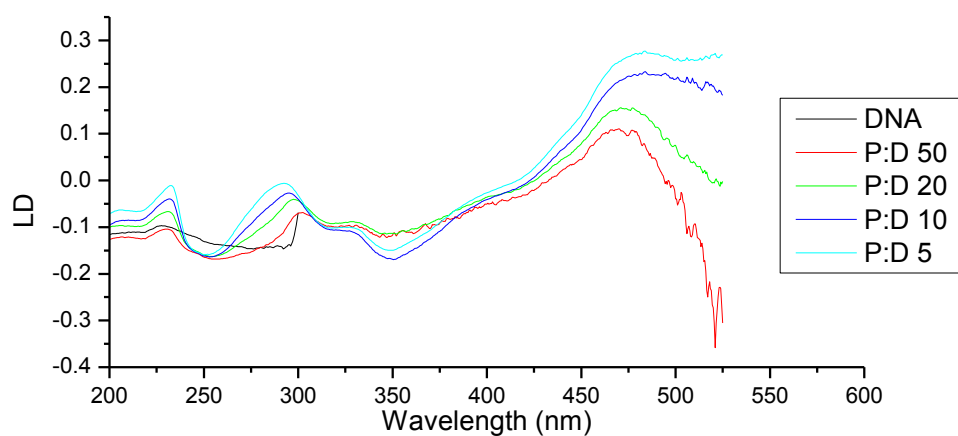


Figure S27: Reduced linear dichroism spectra of st-DNA (400 μM) in 10 mM sodium phosphate buffered aqueous solution at pH 7.4, in the absence and presence of (a) **3** and (b) **4** at different P/D ratios.

d) Thermal denaturation studies

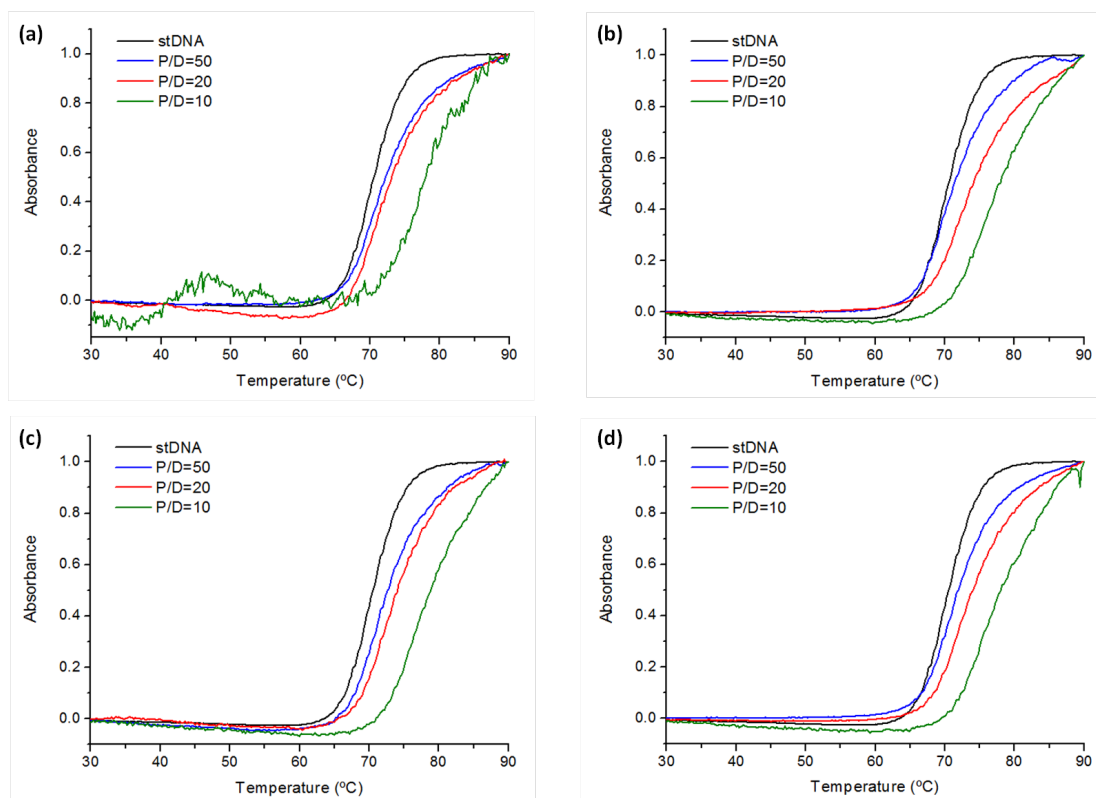


Figure S28: Thermal denaturation curves of st-DNA (150 μM) in 10 mM phosphate buffered aqueous solution at pH 7.4, in the absence and presence of (a) **3**, (b) **4**, (c) **5** and (d) **6** at different P/D ratios.

4. Crystallographic data

Table S4: Crystallographic data.

	6 •2Cl•4H ₂ O	4 •2Cl•xH ₂ O
Chemical formula	C ₃₈ H ₃₂ Cl ₂ N ₁₄ O ₆ RuS	C ₈₂ H ₄₇ Cl ₄ N ₂₈ Ru ₂
Formula mass (g mol ⁻¹)	984.80	1768.42
Crystal system	monoclinic	triclinic
Space group	C2/c	P-1
Crystal size (mm)	0.18 × 0.12 × 0.07	0.22 × 0.12 × 0.08
Cell		
• a (Å)	14.9292(5)	13.41(5)
• b (Å)	14.9340(6)	20.75(7)
• c (Å)	35.2162(12)	21.49(8)
• α (°)	90	63.55(6)
• β (°)	96.717(2)	80.88(6)
• γ (°)	90	88.05(6)
• Volume (Å ³)	7797.7(5)	5282(33)
Z	8	2
Absorption coefficient μ (mm ⁻¹)	5.605	0.436
Reflections		
• total	29550	40313
• unique	4756	10142
Parameters	544	1048
Restraints	37	106
Constraints	0	0
R(int)	0.0603	0.1647
Final refinement values		
• R1 (F ² > σ (F ²))	0.0941	0.0992

• $wR2 (F^2 > \sigma(F^2))$	0.2101	0.2605
• $R1$ (all)	0.1006	0.2165
• $wR2$ (all)	0.2136	0.3361
• Goodness of fit	1.264	1.008
CCDC number	1489207	1489206

Table S5: Selected bond lengths and angles for crystals $4.2\text{Cl}\cdot x\text{H}_2\text{O}$. Distances in Å, angles in degrees.

Bond distance		Angle	
Ru(1)–N(1)	2.036(17)	N(6)–Ru(1)–N(1)	81.5(7)
Ru(1)–N(6)	2.034(15)	N(6)–Ru(1)–N(10)	95.4(6)
Ru(1)–N(7)	2.076(16)	N(6)–Ru(1)–N(7)	88.8(5)
Ru(1)–N(10)	2.12(2)	N(1)–Ru(1)–N(7)	95.0(7)
Ru(1)–N(11)	1.995(18)	N(1)–Ru(1)–N(14)	94.9(6)
Ru(1)–N(14)	2.109(16)	N(7)–Ru(1)–N(10)	79.0(10)
Ru(2)–N(15)	2.078(16)	N(7)–Ru(1)–N(14)	94.3(6)
Ru(2)–N(20)	2.084(14)	N(14)–Ru(1)–N(10)	88.3(5)
Ru(2)–N(21)	2.149(16)	N(11)–Ru(1)–N(6)	95.8(6)
Ru(2)–N(24)	2.085(15)	N(11)–Ru(1)–N(1)	91.3(6)
Ru(2)–N(25)	2.033(18)	N(11)–Ru(1)–N(10)	94.9(10)
Ru(2)–N(28)	2.117(16)	N(11)–Ru(1)–N(14)	81.6(6)
		N(15)–Ru(2)–N(20)	80.8(7)
		N(15)–Ru(2)–N(21)	89.2(5)
		N(15)–Ru(2)–N(24)	93.9(6)
		N(15)–Ru(2)–N(28)	94.5(8)
		N(20)–Ru(2)–N(21)	95.8(6)
		N(20)–Ru(2)–N(28)	89.5(5)
		N(24)–Ru(2)–N(21)	81.9(7)
		N(24)–Ru(2)–N(28)	93.0(6)
		N(25)–Ru(2)–N(20)	93.5(7)
		N(25)–Ru(2)–N(21)	96.6(8)
		N(25)–Ru(2)–N(24)	91.9(5)
		N(25)–Ru(2)–N(28)	80.1(9)

Table S6: Selected bond lengths and angles for crystal $6.2\text{Cl}\cdot 4\text{H}_2\text{O}$. Distances in Å, angles in degrees.

Bond distance		Angle	
Ru(1)–N(1)	2.075(10)	N(10)–Ru(1)–N(7)	82.1(4)
Ru(1)–N(6)	2.067(9)	N(10)–Ru(1)–N(14)	94.9(3)
Ru(1)–N(7)	2.068(10)	N(10)–Ru(1)–N(1)	91.0(4)
Ru(1)–N(10)	2.052(10)	N(10)–Ru(1)–N(6)	91.8(3)
Ru(1)–N(11)	2.060(9)	N(11)–Ru(1)–N(7)	93.8(4)
Ru(1)–N(14)	2.055(9)	N(11)–Ru(1)–N(1)	93.4(3)
S(1)–N(3)	1.613(12)	N(11)–Ru(1)–N(6)	92.9(3)
S(1)–N(4)	1.627(11)	N(14)–Ru(1)–N(7)	89.6(3)
		N(14)–Ru(1)–N(11)	80.7(3)
		N(14)–Ru(1)–N(1)	95.9(3)
		N(6)–Ru(1)–N(7)	95.2(3)
		N(6)–Ru(1)–N(1)	80.1(3)
		N(3)–S(1)–N(4)	100.9(6)

Table S7: Hydrogen bonds for for crystals $4.2\text{Cl}\cdot x\text{H}_2\text{O}$. Distances in Å, angles in degrees.

H bond	dist(DH)	dist(HA)	dist(DA)	angle(DHA)	sym. op. on A
O2–H2A...Cl1	0.80	2.18	2.985(3)	179.9	1-x,1-y,1-z
O3–H3B...O5	0.78	2.11	2.890(19)	179.7	x+1/2, y-1/2, z

O4—H4A...O2	0.86	2.05	2.871(17)	158.3	1-x,1-y,1-z
O4—H4B...O5	0.79	2.22	3.01(2)	179.5	
O6—H6A...O4	0.85	2.01	2.864(19)	174.6	-x+1/2, -y+3/2, 1-z
O6—H6B...N9	0.86	2.09	2.875(16)	150.1	x-1/2, y+1/2, z

References

1. T. Murashima, K.-i. Fujita, K. Ono, T. Ogawa, H. Uno and N. Ono, *Journal of the Chemical Society, Perkin Transactions 1*, 1996, DOI: 10.1039/P19960001403, 1403-1407.
2. X. Hui, F. Schmidt, M. A. Fakhfakh, X. Franck and B. Figadere, *Heterocycles*, 2007, **72**, 353-361.
3. CS104455, 1961.
4. L. Ferrie, B. Figadere, G. Le Douaron, R. Raisman-Vozari and F. Schmidt, *Journal*, 2012.
5. B. A. DaSilveira Neto, A. S. A. Lopes, G. Ebeling, R. S. Gonçalves, V. E. U. Costa, F. H. Quina and J. Dupont, *Tetrahedron*, 2005, **61**, 10975-10982.
6. C. M. Cillo and T. D. Lash, *J. Heterocycl. Chem.*, 2004, **41**, 955-962.
7. P. B. Ghosh and B. J. Everitt, *J Med Chem*, 1974, **17**, 203-206.
8. T. Doi, H. Nagamiya, M. Kokubo, K. Hirabayashi and T. Takahashi, *Tetrahedron*, 2002, **58**, 2957-2963.
9. S. Rau, D. Walther and J. G. Vos, *Dalton Trans.*, 2007, DOI: 10.1039/b615987g, 915-919.
10. A. M. Brouwer, *Pure and Applied Chemistry*, 2011, **83**, 2213-2228.
11. M. T. Carter, M. Rodriguez and A. J. Bard, *Journal of the American Chemical Society*, 1989, **111**, 8901-8911.
12. N. C. Garbett, P. A. Ragazzon and J. B. Chaires, *Nature protocols*, 2007, **2**, 3166-3172.
13. <http://www.originlab.com/originpro>.
14. P. Thordarson, *Chemical Society Reviews*, 2011, **40**, 1305-1323.
15. W. Bujalowski, *Chemical reviews*, 2006, **106**, 556-606.